

# Critical Properties of the Superfluid – Bose Glass Transition in Two Dimensions

Juan Pablo Álvarez Zúñiga, David J. Luitz, Gabriel Lemarié, and Nicolas Laflorencie  
*Laboratoire de Physique Théorique, IRSAMC, Université de Toulouse, CNRS, 31062 Toulouse, France*  
(Dated: December 15, 2014)

We investigate the superfluid (SF) to Bose glass (BG) quantum phase transition using extensive quantum Monte Carlo simulations of two-dimensional hard-core bosons in a random box potential.  $T = 0$  critical properties are studied by thorough finite-size scaling of condensate and SF densities, both vanishing at the same critical disorder  $W_c = 4.80(5)$ . Our results give the following estimates for the critical exponents:  $z = 1.85(15)$ ,  $\nu = 1.20(12)$ ,  $\eta = -0.40(15)$ . Furthermore, the probability distribution of the SF response  $P(\ln \rho_{\text{sf}})$  displays striking differences across the transition: while it narrows with increasing system sizes  $L$  in the SF phase, it broadens in the BG regime, indicating an absence of self-averaging, and at the critical point  $P(\ln \rho_{\text{sf}} + z \ln L)$  is scale invariant. Finally, high-precision measurements of the local density rule out a percolation picture for the SF-BG transition.

*Introduction*—The interplay between disorder and interactions in condensed matter systems, while intensively studied during the last decades, remains today puzzling in many respects for both experimental and theoretical investigations [1]. First raised by experiments in the late 1980s on superfluid  $^4\text{He}$  in porous media [2, 3], the theoretical question of interacting bosons in the presence of disorder has been addressed at the same time by several pioneer works [4–8]. It was then rapidly understood that for two dimensional (2D) bosons with repulsive interaction, superfluidity is robust to weak disorder.

A breakthrough came with the thorough study of the critical properties of the quantum ( $T = 0$ ) phase transition between superfluid (SF) and localized Bose-glass (BG) regimes by Fisher *et al.* [8]. In particular, a generalization of the Josephson scaling relations [9] was given, thus predicting new critical exponents (see first line of Tab. I). Following this work a great endeavour has been made, using exact numerical techniques such as quantum Monte Carlo (QMC) [10–26] or the density matrix renormalization group (DMRG) [27–29], in order to explore in detail the phase diagram of the disordered Bose-Hubbard model. Nevertheless, a general consensus regarding the precise values of the critical exponents at the SF-BG transition is still lacking, despite huge analytical [6, 8, 30–36] and numerical [12–20, 24–26] efforts.

At the same time a wealth of new experiments have been developed, using different techniques and setups: (i) ultracold bosonic atoms in a random potential [37–40]; (ii) strongly disordered superconducting films where preformed Cooper pairs can localize [41–44]; (iii) impurity doped quantum magnets at high field [45–49]. They all have shed a new light on the problem of boson localization but raised important theoretical questions, regarding *e.g.* the precise nature of the critical point [32–35], the inhomogeneous character of the SF and BG phases [41, 42, 50, 51].

In this Letter, we address two important issues of the Bose glass problem using the most advanced available exact numerical technique, namely the stochastic series expansion (SSE) QMC method. The quantum critical

behavior at the onset of boson localization and the delicate estimate of the critical exponents are first discussed. Then the inhomogeneous nature of the SF and BG phases is addressed through the study of the probability distribution of the SF response which shows strikingly different properties when increasing lattice sizes. Shrinking in the SF phase, it clearly broadens in the BG regime, thus indicating the absence of self-averaging [52]. We also demonstrate that all sites remain compressible, ruling out a percolation picture. Our conclusions are supported by careful ground-state (GS) simulations through the so-called  $\beta$ -doubling scheme, disorder averaging over a very large number of realizations, detailed error bar evaluation, and systematic finite-size scaling analysis.

*Model and Quantum Monte Carlo approach*—We consider hard-core bosons at half-filling on a two-dimensional square lattice, described by

$$\mathcal{H} = -t \sum_{\langle ij \rangle} (b_i^\dagger b_j + b_j^\dagger b_i) - \sum_i \mu_i b_i^\dagger b_i, \quad (1)$$

where hopping between nearest neighbours is fixed to  $t = 1/2$ , and the random chemical potential  $\mu_i$  is drawn from a uniform distribution  $[-W, W]$ , *i.e.* half-filling is statistically achieved, on average [53]. This model, also relevant to describe many aspects of strongly disordered superconductors [4, 5, 41, 42, 50, 54], exhibits a quantum ( $T = 0$ ) phase transition between a Bose condensed SF and a localized BG regime at sufficiently strong disorder [13, 15, 19].

The intrinsic difficulties to simulate with QMC methods the low temperature properties of such a strongly disordered quantum system are twofold: (i) accessing ground-state (GS) properties means very long equilibration and simulation times; (ii) statistical uncertainties of the measured physical observables originate from both MC sampling with  $N_{\text{mc}}$  steps and random sample to sample fluctuations with  $\mathcal{N}_s$  samples. Therefore, the simulation time grows very fast as  $L^2 \times \beta \times N_{\text{mc}} \times \mathcal{N}_s$  which limits the largest system size  $L$  reachable. The strategy we adopt to tackle this problem, using the SSE algorithm [55], is as follows (simulation details are discussed

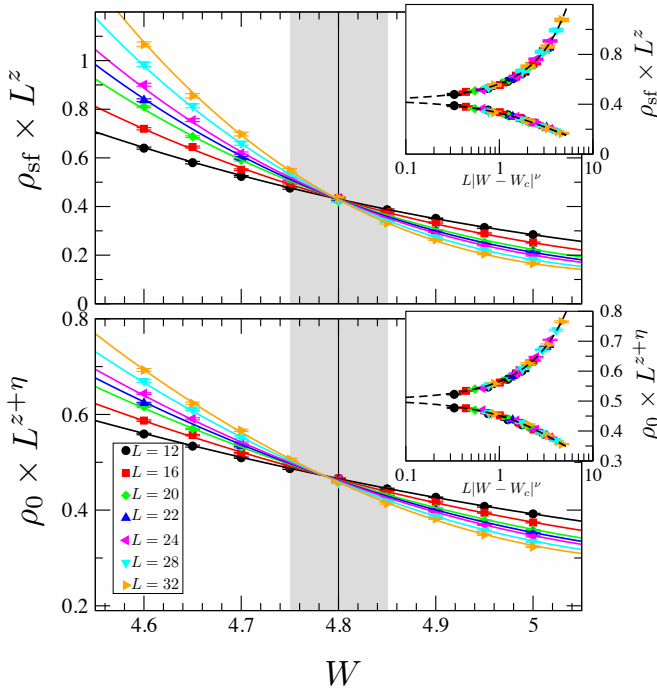


Figure 1. Scaling analysis of the SF  $\rho_{\text{sf}}$  (top) and BEC  $\rho_0$  (bottom) densities. Solid lines show best fits to the universal scaling functions Eqs. (2) and (3) for the full data set with  $z \simeq 1.85$ ,  $W_c^{\text{sf}} \simeq 4.8$ ,  $W_c^0 \simeq 4.79$ ,  $z + \eta \simeq 1.42$ ,  $\nu_{\text{sf}} \simeq 1.1$ ,  $\nu_0 \simeq 1.2$ , and  $\mathcal{G}_{\text{sf}|0}$  3<sup>rd</sup> order polynomials. The distance from the critical point  $W_c = 4.80(5)$  (grey area), when rescaled by  $L^{-1/\nu}$  with  $\nu = 1.2$ , yields a perfect data collapse (insets).

in the supplementary material [56]). First we use the  $\beta$ -doubling scheme to speed up equilibration towards very low temperature [56–58], after what we perform for each sample a number of measurement steps  $N_{\text{mc}}^s$  (sample dependent) large enough that the SF density is efficiently measured [56]. This procedure is then repeated for a very large number of disorder realizations  $\mathcal{N}_s = \mathcal{O}(10^4)$ . We have noticed that GS convergence is in practice extremely hard to achieve rigorously for all samples, as some samples may exhibit finite-size gaps smaller than the infrared cutoff of the  $\beta$ -doubling expansion, which is fixed on average. Nevertheless, we have checked that intrinsic MC errors induced by such a slow GS convergence remain smaller than statistical errors. The results, at  $\beta t = 2^h$  with  $h = 7$  for  $L = 12$  up to  $h = 9$  for the largest sizes, can therefore be safely interpreted as  $T = 0$  ones [56].

*Finite-size scaling*—Motivated by the fact that previous works disagree on the values of the critical parameters (see [13, 15, 19] and Tab. I), we now discuss our determination of these parameters by the finite-size scaling approach for disorder averaged QMC estimates of the SF and Bose condensed densities.

The ordered regime is characterized by a finite SF density  $\rho_{\text{sf}}$ , efficiently estimated using the winding number

fluctuations in the QMC algorithm [59]. In the vicinity of the 2D quantum critical point, the finite-size scaling of the SF density is

$$\rho_{\text{sf}}(L) = L^{-z} \mathcal{G}_{\text{sf}}[L^{1/\nu}(W - W_c)], \quad (2)$$

where  $z$  is the dynamical critical exponent,  $\nu$  the correlation length exponent,  $W_c$  the critical disorder, and  $\mathcal{G}_{\text{sf}}$  a universal function.

Beyond the SF response, one can also probe Bose-Einstein condensation (BEC), occurring in 2D at  $T = 0$  where U(1) symmetry can be broken. The BEC density  $\rho_0 = \sum_{ij} G_{ij}/N^2$ , obtained from the equal time Green’s function [60]  $G_{ij} = \langle b_i^\dagger b_j \rangle$ , plays the role of the order parameter, with a critical scaling

$$\rho_0(L) = L^{-z-\eta} \mathcal{G}_0[L^{1/\nu}(W - W_c)]. \quad (3)$$

Our QMC data are very nicely described by the above scaling forms, as shown in Fig. 1 for both SF and BEC densities. Strikingly, BEC and SF densities vanish at the same disorder strength  $W_c = 4.80(5)$ . The values of the critical exponents are given in Table I. This determination results from fits of our data set by Taylor expanding the scaling functions  $\mathcal{G}_{\text{sf}}$  and  $\mathcal{G}_0$  around  $W_c$  up to an order large enough that the goodness of fit is acceptable (3rd order in Fig. 1, see [56]). We have performed a careful error analysis using the bootstrap approach in order to estimate statistical errors of the fit parameters, as well as potential systematic errors by fitting over various ranges of disorder strengths and sizes [56]. This results in conservative uncertainties for the estimates of the critical parameters, as visible in Tab. I.

We observe a good agreement with the predicted bounds from Fisher *et al.* [8] for  $\nu = 1.20(12) \geq 1$  and  $\eta = -0.40(15) \leq 0$ . Regarding the more debated question of the dynamical exponent [32], while still compatible with  $z = 2$  within error bars our best estimate gives a smaller number  $z = 1.85(15)$ , in agreement with a recent careful estimate for quantum rotors [25]. Comparing with other studies in Tab. I, our results, obtained with much larger system sizes, agree within error bars with Ref. [15], whereas results in Refs. [13, 19] are probably biased due to finite temperature effects and too small disorder averaging.

$z$	$\nu$	$\eta$	$W_c$	Reference
2	$\geq 1$	$\leq 0$		Fisher <i>et al.</i> [8]
0.5(1)	2.2(2)	n.a.	2.5	Makivić <i>et al.</i> [13]
2.0(4)	0.90(13)	n.a.	4.95(20)	Zhang <i>et al.</i> [15]
1.40(2)	1.10(4)	-0.22(6)	4.42(2)	Priyadarshie <i>et al.</i> [19]
1.85(15)	1.20(12)	-0.40(15)	4.80(5)	This work

Table I. Various estimates of critical exponents and disorder strength  $W_c$  for the 2D SF–BG transition of model Eq. (1).

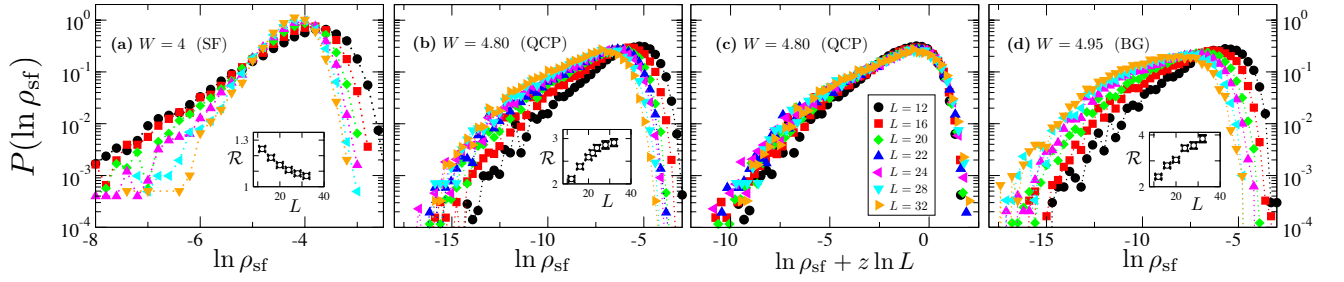


Figure 2. Histogram of QMC estimates for  $\ln \rho_{\text{sf}}$  performed over  $\mathcal{N}_s \sim 10^4$  disordered samples for each size  $L$ . (a) In the SF regime  $W = 4$ , distributions get narrower with increasing  $L$  whereas in the BG phase (d) for  $W = 4.95$  they broaden. At criticality  $W_c = 4.8$  (b-c) the broadening stops above  $L = 20$  and  $P(\ln \rho_{\text{sf}} + z \ln L)$  displays a good collapse using  $z = 1.85$ . The insets show the ratio  $\mathcal{R} = \rho_{\text{sf}}^{\text{avg}} / \rho_{\text{sf}}^{\text{typ}}$  vs. system size  $L$ .

*Distributions and absence of self-averaging in the BG*— In order to go beyond the analysis of the critical properties based on disorder averaged observables, we now turn to the much less studied issue of distributions. The question of a possible broadening of the responses, linked to the issue of self-averaging, has not been studied for 2D bosons, although it may be crucial as discussed for disordered Ising models [61–63] and strongly disordered superconductors [41, 42, 50]. Here we focus on the probability distribution  $P(\ln \rho_{\text{sf}})$ , obtained by building histograms of QMC estimates for  $\ln \rho_{\text{sf}}$  over  $\mathcal{N}_s$  independent samples, with  $\mathcal{N}_s \approx 2 \times 10^4$  for  $L \leq 22$  and  $\mathcal{N}_s \approx 10^4$  for  $L \geq 24$ , shown in Fig. 2 for three values of the disorder strength.

In the SF regime (panel (a)  $W = 4 < W_c$ ) the distribution narrows upon increasing the size  $L$ , thus demonstrating that the SF response is self-averaging in the ordered phase. Conversely, as visible in panel (d) for the BG regime at  $W = 4.95 > W_c$ ,  $P(\ln \rho_{\text{sf}})$  broadens when  $L$  increases, and moves towards large negative values, as expected in the thermodynamic limit where the SF stiffness vanishes. We therefore expect a difference between average and typical SF densities in the BG: as shown in the insets of Fig. 2, the ratio  $\mathcal{R} = \rho_{\text{sf}}^{\text{avg}} / \rho_{\text{sf}}^{\text{typ}}$  clearly increases with  $L$  in the BG regime (d) whereas it goes to 1 in the SF phase (a). At the critical point  $W_c = 4.8$  (panels (b-c) of Fig. 2), the histograms first broaden for small sizes and then, above  $L = 20$  the curves appear self-similar, simply shifted relative to each other. This absence of broadening at large scales is also visible in the inset (b) where the ratio  $\mathcal{R}$  tends to saturate to a constant value. The shift of the distributions can be corrected for by adding  $z \ln L$  to  $\ln \rho_{\text{sf}}$  using our best estimate  $z = 1.85$ . Indeed, as shown in Fig. 2 (c)  $P[\ln(L^z \rho_{\text{sf}})]$  yields a collapse onto a scale invariant distribution, particularly good above  $L = 20$ .

The fact that all distributions at  $W_c$  are identical up to a shift suggests that, while typical and average SF densities scale differently in the BG regime, their critical scalings are described by the same exponents. Indeed, the typical SF density, defined as  $\rho_{\text{sf}}^{\text{typ}} = \exp(\ln \rho_{\text{sf}})$  (where  $\langle \dots \rangle$  stands for disorder averaging), can be analyzed using a scaling hypothesis similar to the average Eq. (2),

but including additional irrelevant corrections [64]

$$\rho_{\text{sf}}^{\text{typ}}(L) = L^{-z} \left( \mathcal{G}_{\text{sf}}^{\text{typ}} [L^{1/\nu} (W - W_c)] + cL^{-y} \right). \quad (4)$$

Because of the presence of irrelevant corrections, a fit of our data set by Eq. (4) with a polynomial  $\mathcal{G}_{\text{sf}}$  is unstable unless we fix the critical parameters  $W_c$ ,  $z$  and  $\nu$  to our best estimates (Tab. I). The crossing of  $\rho_{\text{sf}}^{\text{typ}} \times L^z$  vs  $W$  plotted in Fig. 3 (a) displays a non-negligible drift, well captured by irrelevant corrections in Eq. (4) with  $y = 0.97(4)$ . A nice way to achieve a scaling plot for the typical SF density is then to divide  $\rho_{\text{sf}}^{\text{typ}}$  by its value at  $W_c$ , this in order to cancel out the irrelevant corrections  $\sim L^{-y}$ . Next, a rescaling of the length  $L$  by the correlation length  $\xi = |W - W_c|^{-\nu}$  with  $\nu = 1.2$  and  $W_c = 4.8$ , gives an almost perfect collapse, without any additional adjustable parameters, as shown in

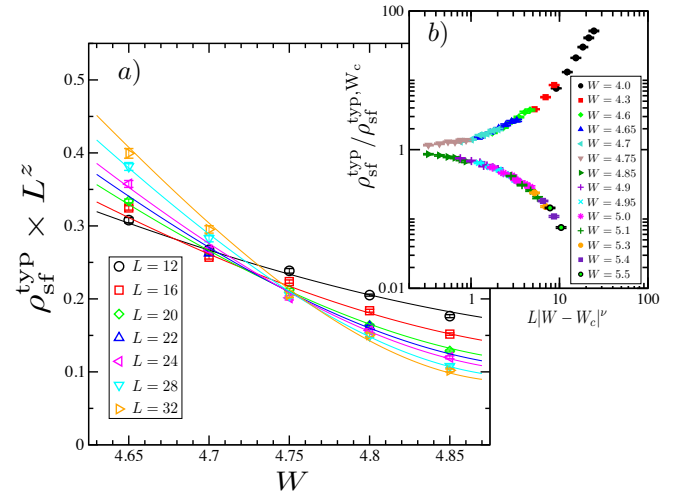


Figure 3. Typical SF density (a) plotted as  $\rho_{\text{sf}}^{\text{typ}} \times L^z$  vs.  $W$  where the crossing at  $W_c = 4.8$  has a visible drift, captured by  $\mathcal{G}_{\text{sf}}^{\text{typ}} [L^{1/\nu} (W - W_c)] + cL^{-y}$  with fixed  $\nu = 1.2$  and  $z = 1.85$ , and an estimated irrelevant exponent  $y = 0.97(4)$ . In panel (b),  $\rho_{\text{sf}}^{\text{typ}} / \rho_{\text{sf}}^{\text{typ}, W_c}$  plotted against  $L|W - W_c|^\nu$  exhibits an almost perfect collapse of the data for  $4 \leq W \leq 5.5$  and  $12 \leq L \leq 32$  with no additional parameters.

Fig. 3 (b) for  $4.0 \leq W \leq 5.5$  and all available system sizes  $12 \leq L \leq 32$ . This demonstrates that the quantum critical behaviours of average and typical SF densities are similar, in particular their critical exponents  $z_{\text{avg}} = z_{\text{typ}} = 1.85(15)$  and  $\nu_{\text{typ}} = \nu_{\text{avg}} = 1.20(12)$ .

Coming back to the distributions, the drift observed for the typical stiffness in Fig. 3 (a) is related to the transient (irrelevant) broadening of  $P(\ln \rho_{\text{sf}})$  observed at small sizes in Fig. 2 (b). In order to take such a crossover into account and get rid of irrelevant corrections, we study the broadening of  $P(\ln \rho_{\text{sf}})$  using the corrected standard deviation (StD)  $\tilde{\sigma}_{\ln \rho_{\text{sf}}} = \sigma_{\ln \rho_{\text{sf}}} - \sigma^c$ , where  $\sigma^c$  is the StD at criticality. This is plotted in Fig. 4 vs.  $L|W - W_c|^\nu = L/\xi$ , where a very good collapse of the data is achieved without any adjusted parameters. In the SF regime,  $\tilde{\sigma}$  converges towards  $-\sigma^c$  as  $1/\sqrt{N}$  (dashed curve), a consequence of self-averaging. More interestingly, the BG phase features an opposite qualitative behavior with  $\tilde{\sigma}$  growing with system size, as  $(L/\xi)^\omega$  (full line). A careful study of such very broad distributions hits the limits of our numerics, leading to quite large statistical errors, despite the very large number of samples  $\mathcal{N}_s = \mathcal{O}(10^4)$ , but nevertheless allows to estimate the exponent  $\omega = 0.5(2)$ . We interpret this result as follows: The prediction [54] that the stiffness is dominated by quasi 1D paths suggests that one may understand the global SF response  $\rho_{\text{sf}}$  as a purely local quantity in the BG insulator. Moreover, an analogy [42, 50] between the BG and the disordered phase of the random transverse-field Ising model [61], as supported by recent 1D results [65], suggests that the BG is governed by directed-polymer physics in dimension  $1+1$  [66]. This predicts an exponent  $\omega = 1/3$  [67] for local quantities which is compatible with our estimate.

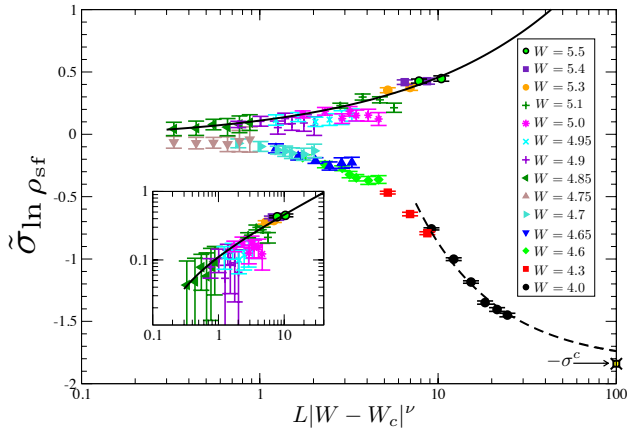


Figure 4. Corrected standard deviation of the logarithm of the SF response  $\tilde{\sigma}_{\ln \rho_{\text{sf}}} = \sigma_{\ln \rho_{\text{sf}}} - \sigma^c$  vs. system size in units of the typical length scale  $\xi = |W - W_c|^{-\nu}$ . In the SF phase  $W < 4.8$ ,  $\tilde{\sigma}$  tends to  $-\sigma^c$  as  $1/L$  (dashed line), whereas in the BG regime  $W > 4.8$ ,  $\tilde{\sigma}$  grows as  $L^\omega$  (full black line) with  $\omega = 0.5(2)$ . Inset: zoom on the BG regime.

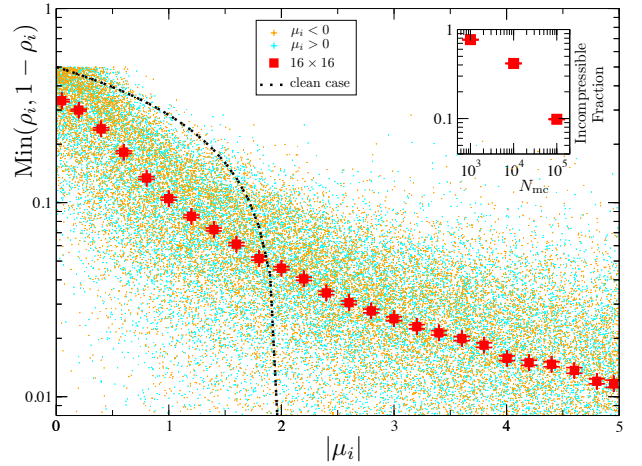


Figure 5. Local particle (hole) densities  $\rho_i$  ( $1 - \rho_i$ ) plotted vs. local chemical potentials  $|\mu_i|$ . Small blue (orange) points show QMC results of  $\mathcal{N}_s = 150$  samples of size  $16 \times 16$  measured at  $\beta t = 1024$  with  $N_{\text{mc}} = 10^5$  steps. The red data points show averages over windows of the chemical potential of size  $\bar{\mu} - 0.1 \leq \mu_i \leq \bar{\mu} + 0.1$  and the clean ( $W = 0$ ) result is shown by the dashed line, yielding exactly zero for  $|\mu| > 2$  for  $\text{Min}(\rho_i, 1 - \rho_i)$  [68]. The inset quantifies the incompressible fraction, *i.e.* the fraction of sites with  $\rho_i = 0$  or  $\rho_i = 1$  as a function of MC steps showing that in the exact limit of infinite Markov chains the incompressible fraction tends to zero.

*Local density and absence of percolation*— Finally, we want to discuss some microscopic properties of the insulating BG state. For this we focus on the local bosonic density  $\rho_i = \langle b_i^\dagger b_i \rangle$ , shown in Fig. 5 in the BG regime ( $W = 5$ ) for  $16 \times 16$ , at low enough temperature  $\beta t = 1024$  such that the total number of bosons does not fluctuate (see [56]). Clearly, the average behavior is always compressible, which contrasts with the clean case where the system is incompressible whenever  $|\mu| > 2$  [68]. Furthermore, the fraction of incompressible sites with  $\rho_i = 0$  or  $1$  decreases with the number of MC steps and seems to vanish in the exact limit (inset). This shows that percolation through compressible sites is present even in the BG phase, at least from such a single particle view, and is therefore not related to the SF-BG transition, in contrast with some recent discussions [51, 69].

*Conclusions*— Large-scale QMC simulations of the SF-BG transition supplemented by finite-size scaling show that SF and BEC densities disappear at the same critical disorder strength  $W_c \approx 4.8$ , with critical exponents  $z \approx 1.85$ ,  $\nu \approx 1.2$ , and  $\eta \approx -0.4$ . The SF density distribution becomes infinitely broad upon increasing system size in the BG insulator, a characteristic signature of the absence of self-averaging supporting the fact that the SF density is a purely local quantity at strong disorder. Our results also rule out a classical percolation scenario of incompressible sites in the BG.



This work was performed using HPC resources from GENCI (grant x2014050225) and CALMIP (grant 2014-P0677), and is supported by the French ANR program ANR-11-IS04-005-01 and by the label NEXT. During the completion of this study we became aware of a parallel work [70], which reaches comparable conclusions.

- 
- [1] T. Giamarchi, *Comptes Rendus Physique* **14**, 637 (2013).
  - [2] D. Finotello, K. A. Gillis, A. Wong, and M. H. W. Chan, *Phys. Rev. Lett.* **61**, 1954 (1988).
  - [3] J. D. Reppy, *J Low Temp Phys* **87**, 205 (1992).
  - [4] M. Ma and P. A. Lee, *Phys. Rev. B* **32**, 5658 (1985).
  - [5] M. Ma, B. I. Halperin, and P. A. Lee, *Phys. Rev. B* **34**, 3136 (1986).
  - [6] T. Giamarchi and H. J. Schulz, *EPL* **3**, 1287 (1987).
  - [7] D. S. Fisher and M. P. A. Fisher, *Phys. Rev. Lett.* **61**, 1847 (1988).
  - [8] M. P. A. Fisher, P. B. Weichman, G. Grinstein, and D. S. Fisher, *Phys. Rev. B* **40**, 546 (1989).
  - [9] B. D. Josephson, *Physics Letters* **21**, 608 (1966).
  - [10] W. Krauth, N. Trivedi, and D. Ceperley, *Phys. Rev. Lett.* **67**, 2307 (1991).
  - [11] R. T. Scalettar, G. G. Batrouni, and G. T. Zimanyi, *Phys. Rev. Lett.* **66**, 3144 (1991).
  - [12] E. S. Sørensen, M. Wallin, S. M. Girvin, and A. P. Young, *Phys. Rev. Lett.* **69**, 828 (1992).
  - [13] M. Makivić, N. Trivedi, and S. Ullah, *Phys. Rev. Lett.* **71**, 2307 (1993).
  - [14] P. B. Weichman, *Phys. Rev. Lett.* **74**, 1038 (1995).
  - [15] S. Zhang, N. Kawashima, J. Carlson, and J. E. Gubernatis, *Phys. Rev. Lett.* **74**, 1500 (1995).
  - [16] J. Kisker and H. Rieger, *Phys. Rev. B* **55**, R11981 (1997).
  - [17] F. Alet and E. S. Sørensen, *Phys. Rev. E* **67**, 015701 (2003).
  - [18] N. Prokof'ev and B. Svistunov, *Phys. Rev. Lett.* **92**, 015703 (2004).
  - [19] A. Priyadarshree, S. Chandrasekharan, J.-W. Lee, and H. U. Baranger, *Phys. Rev. Lett.* **97**, 115703 (2006).
  - [20] P. Hitchcock and E. S. Sørensen, *Phys. Rev. B* **73**, 174523 (2006).
  - [21] V. Gurarie, L. Pollet, N. V. Prokof'ev, B. V. Svistunov, and M. Troyer, *Phys. Rev. B* **80**, 214519 (2009).
  - [22] J. Carrasquilla, F. Becca, A. Trombettoni, and M. Fabrizio, *Phys. Rev. B* **81**, 195129 (2010).
  - [23] F. Lin, E. S. Sørensen, and D. M. Ceperley, *Phys. Rev. B* **84**, 094507 (2011).
  - [24] S. Söyler, M. Kiselev, N. V. Prokof'ev, and B. V. Svistunov, *Phys. Rev. Lett.* **107**, 185301 (2011).
  - [25] H. Meier and M. Wallin, *Phys. Rev. Lett.* **108**, 055701 (2012).
  - [26] Z. Yao, K. P. C. da Costa, M. Kiselev, and N. Prokof'ev, *Phys. Rev. Lett.* **112**, 225301 (2014).
  - [27] R. V. Pai, R. Pandit, H. R. Krishnamurthy, and S. Ramasesha, *Phys. Rev. Lett.* **76**, 2937 (1996).
  - [28] S. Rapsch, U. Schollwöck, and W. Zwerger, *EPL* **46**, 559 (1999).
  - [29] G. Roux, T. Barthel, I. McCulloch, C. Kollath, U. Schollwöck, and T. Giamarchi, *Phys. Rev. A* **78**, 023628 (2008).
  - [30] K. G. Singh and D. S. Rokhsar, *Phys. Rev. B* **46**, 3002 (1992).
  - [31] I. F. Herbut, *Phys. Rev. Lett.* **79**, 3502 (1997).
  - [32] P. B. Weichman and R. Mukhopadhyay, *Phys. Rev. Lett.* **98**, 245701 (2007).
  - [33] E. Altman, Y. Kafri, A. Polkovnikov, and G. Refael, *Phys. Rev. B* **81**, 174528 (2010).
  - [34] Z. Ristivojevic, A. Petković, P. Le Doussal, and T. Giamarchi, *Phys. Rev. Lett.* **109**, 026402 (2012).
  - [35] S. Iyer, D. Pekker, and G. Refael, *Phys. Rev. B* **85**, 094202 (2012).
  - [36] J. P. Álvarez Zúñiga and N. Laflorencie, *Phys. Rev. Lett.* **111**, 160403 (2013).
  - [37] M. White, M. Pasienski, D. McKay, S. Q. Zhou, D. Ceperley, and B. DeMarco, *Phys. Rev. Lett.* **102**, 055301 (2009).
  - [38] B. Deissler, M. Zaccanti, G. Roati, C. D'Errico, M. Fattori, M. Modugno, G. Modugno, and M. Inguscio, *Nat Phys* **6**, 354 (2010).
  - [39] S. Krinner, D. Stadler, J. Meineke, J.-P. Brantut, and T. Esslinger, *Phys. Rev. Lett.* **110**, 100601 (2013).
  - [40] C. D'Errico, E. Lucioni, L. Tanzi, L. Gori, G. Roux, I. P. McCulloch, T. Giamarchi, M. Inguscio, and G. Modugno, *Phys. Rev. Lett.* **113**, 095301 (2014).
  - [41] B. Sacépé, T. Dubouchet, C. Chapelier, M. Sanquer, M. Ovadia, D. Shahar, M. Feigel'man, and L. Ioffe, *Nat Phys* **7**, 239 (2011).
  - [42] G. Lemarié, A. Kamlapure, D. Bucheli, L. Benfatto, J. Lorenzana, G. Seibold, S. C. Ganguli, P. Raychaudhuri, and C. Castellani, *Phys. Rev. B* **87**, 184509 (2013).
  - [43] E. Driessen, P. Coumou, R. Tromp, P. de Visser, and T. Klapwijk, *Phys. Rev. Lett.* **109**, 107003 (2012).
  - [44] M. Mondal, A. Kamlapure, S. C. Ganguli, J. Jesudasan, V. Bagwe, L. Benfatto, and P. Raychaudhuri, *Sci. Rep.* **3**, 2013 (2013).
  - [45] T. Hong, A. Zheludev, H. Manaka, and L.-P. Regnault, *Phys. Rev. B* **81**, 060410 (2010).
  - [46] D. Hüvonen, S. Zhao, M. Månsson, T. Yankova, E. Ressouche, C. Niedermayer, M. Laver, S. N. Gvasaliya, and A. Zheludev, *Phys. Rev. B* **85**, 100410 (2012).
  - [47] R. Yu, L. Yin, N. S. Sullivan, J. S. Xia, C. Huan, A. Paduan-Filho, N. F. Oliveira Jr, S. Haas, A. Steppke, C. F. Miclea, F. Weickert, R. Movshovich, E.-D. Mun, B. L. Scott, V. S. Zapf, and T. Roscilde, *Nature* **489**, 379 (2012).
  - [48] M. Vojta, *Phys. Rev. Lett.* **111**, 097202 (2013).
  - [49] A. Zheludev and T. Roscilde, *Comptes Rendus Physique* **14**, 740 (2013).
  - [50] M. V. Feigel'man, L. B. Ioffe, and M. Mézard, *Phys. Rev. B* **82**, 184534 (2010).
  - [51] S. Krinner, D. Stadler, J. Meineke, J.-P. Brantut, and T. Esslinger, *arXiv:1311.5174* (2013).
  - [52] A. Hegg, F. Krüger, and P. W. Phillips, *Phys. Rev. B* **88**, 134206 (2013).
  - [53] P. B. Weichman and R. Mukhopadhyay, *Phys. Rev. B* **77**, 214516 (2008).
  - [54] G. Seibold, L. Benfatto, C. Castellani, and J. Lorenzana, *Phys. Rev. Lett.* **108**, 207004 (2012).
  - [55] O. F. Syljuåsen and A. W. Sandvik, *Phys. Rev. E* **66**, 046701 (2002).
  - [56] See supplementary Material.
  - [57] A. W. Sandvik, *Phys. Rev. B* **66**, 024418 (2002).

- [58] N. Laflorencie, S. Wessel, A. Läuchli, and H. Rieger, *Phys. Rev. B* **73**, 060403 (2006).
- [59] E. Pollock and D. Ceperley, *Phys. Rev. B* **36**, 8343 (1987).
- [60] A. Dorneich and M. Troyer, *Phys. Rev. E* **64**, 066701 (2001).
- [61] D. S. Fisher, *Phys. Rev. B* **51**, 6411 (1995).
- [62] A. P. Young and H. Rieger, *Phys. Rev. B* **53**, 8486 (1996).
- [63] S. Wiseman and E. Domany, *Phys. Rev. Lett.* **81**, 22 (1998).
- [64] A. Rodriguez, L. J. Vasquez, K. Slevin, and R. A. Römer, *Phys. Rev. B* **84**, 134209 (2011).
- [65] H. Javan Mard, J. A. Hoyos, E. Miranda, and V. Dobrosavljević, *Phys. Rev. B* **90**, 125141 (2014).
- [66] C. Monthus and T. Garel, *Journal of Physics A: Mathematical and Theoretical* **45**, 095002 (2012).
- [67] D. Huse, C. Henley, and D. Fisher, *Phys. Rev. Lett.* **55**, 2924 (1985).
- [68] T. Coletta, N. Laflorencie, and F. Mila, *Phys. Rev. B* **85**, 104421 (2012).
- [69] A. E. Niederle and H. Rieger, *New Journal of Physics* **15**, 075029 (2013).
- [70] R. Ng and E. S. Sørensen (preprint).

## SUPPLEMENTARY MATERIAL

This supplementary material provides additional information about our results and details the simulation and data analysis methods. We discuss in detail how finite temperature QMC results are used to access ground-state information, how we perform our careful error analysis and how we extract our best estimates for the critical exponents of the transition. We also analyze the problem of large autocorrelation times for the superfluid density in the Bose glass phase.

### I. $\beta$ -DOUBLING SCHEME AND GROUND-STATE CONVERGENCE

The stochastic series expansion (SSE) being a finite temperature method, it is important to perform calculations at low enough temperatures to capture ground state (GS) properties. In order to accurately study this GS convergence, we have used the  $\beta$ -doubling scheme [1] which consists in performing simulations at exponentially decreasing temperatures by doubling the inverse temperature  $\beta$  as long as we still see a change of the disorder average between the two previous temperatures.

This  $\beta$ -doubling trick allows us to determine the inverse temperature  $\beta t$  at which we should perform the simulations for every system size and every disorder strength in order to ensure that we are really investigating the GS properties. In Fig. 6 we show for two disorder strengths:  $W = 4$  in the superfluid (SF) and  $W = 5$  in the Bose

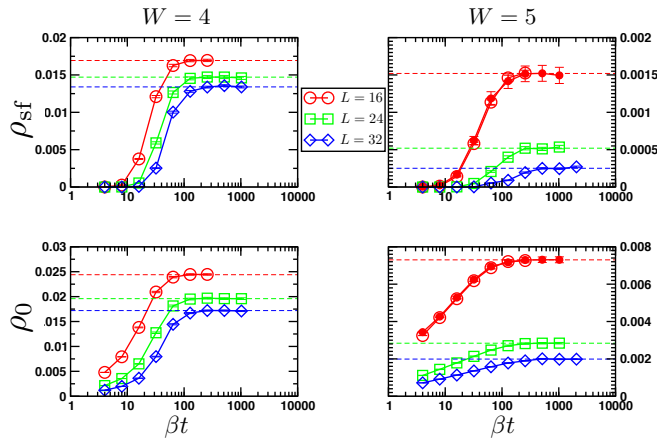


Figure 6. Disorder average of  $\rho_{\text{sf}}$  (top) and  $\rho_0$  (bottom) as a function of inverse temperature  $\beta t$  for different disorder strengths and system sizes. Open symbols are for simulations with  $N_{\text{mc}} = 10^3$  Monte Carlo steps and filled symbols ( $L = 16, W = 5$ ) for  $N_{\text{mc}} = 10^4$  Monte Carlo steps. The averages for different number of MC steps are in full agreement. The average densities saturate to their  $T = 0$  value (indicated by the dashed lines) at a finite  $\beta t$  which will be used to perform the production ground-state simulations.

glass (BG) results of  $\beta$ -doublings for SF and BEC densities, both averaged over  $\sim 10^3$  random samples for three system sizes ( $L = 16, 24, 32$ ). We nicely see that GS-converged expectation values are reached when saturation is achieved. From this  $\beta$ -doubling study, we have fixed for the production simulations  $\beta t = 2^7$  for  $L = 12$  and up to  $\beta t = 2^9$  for  $L = 32$  to study the quantum ( $T = 0$ ) superfluid - Bose glass phase transition.

It is worth noticing that in the right panel of Fig. 6 we also show the  $\beta$ -doubling data for  $L = 16$  and  $W = 5$  with a bigger number of MC steps,  $N_{\text{mc}} = 10^4$ , which are in perfect agreement with the results for  $N_{\text{mc}} = 10^3$ . This feature will be further discussed below.

Note that the  $\beta$ -doubling scheme can be implemented efficiently in SSE by replicating (and inverting) the operator string at inverse temperature  $\beta t$  to obtain an operator string twice as long as an efficient starting point at the inverse temperature  $2\beta t$ , thus minimizing the equilibration time of the Markov chain at  $2\beta t$ . This method is also used to speed up the thermalization process for all our production runs.

Nevertheless, the notion of GS convergence appears to be quite subtle when monitoring various observables. Indeed, the temperature at which a given disordered sample is effectively in its GS, *i.e.* below the finite size gap, is strongly tied to the disorder realization, and contributions from low energy excited states depend on the physical observable which is measured. For example, the total number of particles  $N_{\text{bosons}} = \langle \sum_i n_i \rangle$  is a good quantum number and therefore has to be locked in the GS to an integer number. In the Bose glass (BG) regime, where very small finite size gaps are expected, the histogram of  $N_{\text{bosons}}$  obtained over several hundreds of samples slowly evolves when varying the temperature towards a collection of  $\delta$ -peaks, but only for very large  $\beta$ , as shown in Fig. 7 (right panel). Interestingly, the fraction of samples that are not fully converged to their GS (inset of Fig. 7 right), as far as the total number of bosons is concerned, remain sizeable while the disorder average superfluid (SF) or Bose-Einstein condensate (BEC) densities appear well converged to their  $T = 0$  values, as shown in the left panel of Fig. 7. There we see that for  $N = 8 \times 8$ , the average SF and BEC densities appear converged in temperature for  $\beta t \geq 128$  while the actual fraction of samples with  $N_{\text{bosons}}$  locked is less than 30% for  $\beta t = 128$ .

BEC and SF densities converge much faster to their  $T = 0$  values than  $N_{\text{bosons}}$ . This undoubtedly facilitates the GS simulations as we can stop the  $\beta$  cooling procedure at not too large inverse temperature, as far as SF and BEC densities are concerned. Nevertheless, one should still pay attention to potential systematic bias that may be introduced by rare disorder realizations that may have not fully converged to their GS values for  $\rho_{\text{sf}}$  and  $\rho_0$ . To do so, we fit the  $\beta$ -doubling curves of  $\rho_{\text{sf}}$ —

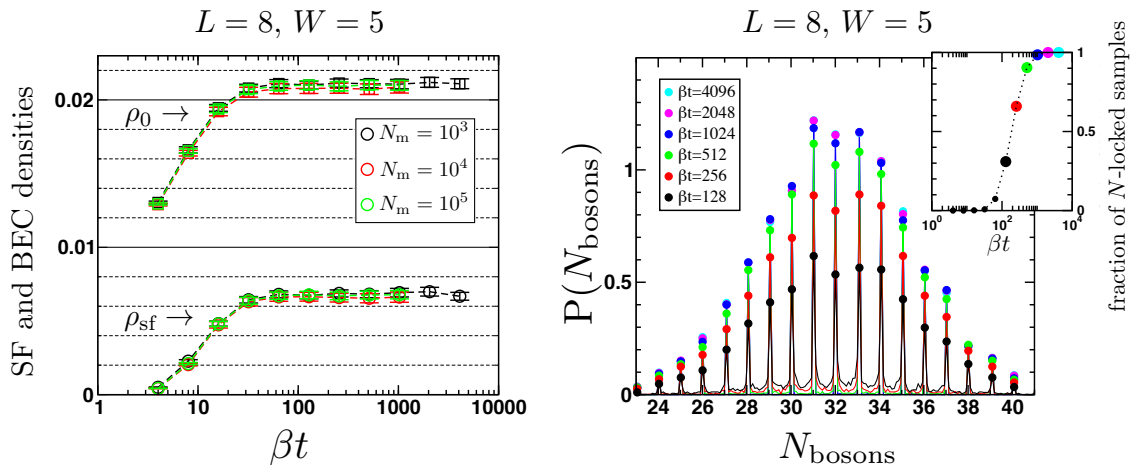


Figure 7. Left panel: Disorder averaged  $\rho_{\text{sf}}$  and  $\rho_0$  as a function of inverse temperature  $\beta t$  for different number of Monte Carlo steps  $N_{\text{MC}}$  for a system of size  $N = 8 \times 8$  at disorder strength  $W = 5$ , averaged over several hundreds of samples. The curves for different number of MC steps are in full agreement. Right panel: particle number histogram for several hundreds of disorder realizations and different temperatures for systems size  $N = 8 \times 8$ . The inset shows the fraction of disorder samples that are actually locked in a sector of fixed number of bosons as a function of the inverse temperature.

as a function of temperature to the following form

$$\rho_{\text{sf}|0}(\beta) = \rho_{\text{sf}|0}(\beta \rightarrow \infty) - A_{\text{sf}|0} \exp(-\beta/\beta_{\text{sf}|0}), \quad (5)$$

which turns out to describe quite well our results with the following fitting parameters

$$\begin{cases} A_{\text{sf}} \approx \frac{2}{L^2}, \\ A_0 \approx \frac{1}{L^2}, \\ \beta_{\text{sf}} = \beta_0 \approx 0.1L^2. \end{cases} \quad (6)$$

With this simple phenomenological description, we have checked the stability of our scaling analysis, and concluded that our results do not change upon the inclusion of such a correction term (see Fig. 12). Note that the correction is small enough so that the corrected result is still within the error bar as guaranteed by our convergence check in Fig. 6.

## II. ERROR BARS AND EVALUATION OF SYSTEMATIC ERRORS

Monte Carlo (MC) results for disordered systems have two sources of statistical errors: (i) Statistical fluctuations of the Monte Carlo result for each random sample, which can be reduced by generating longer Markov chains. (ii) Statistical fluctuations of the disorder average over random samples which can be reduced by including more realizations.

### A. MC error vs. disorder fluctuations

It is crucial to distribute the available computer time efficiently over the different competing tasks (large  $\beta$ , number of MC steps, number of random samples) in order to maximize the overall precision. Therefore, we compare the MC error bar to the error bar stemming from disorder averaging. We choose a minimal number of 1000 MC measurements in order to assure that the Markov chain is much longer than the autocorrelation times of  $\rho_0$  and  $\rho_{\text{sf}}$  and it is not allowed to perform less MC steps as this leads to wrong results and introduces a systematic error.

Figure 8 shows clearly that MC fluctuations within one disorder realization are much smaller than the error bar stemming from the fluctuations between disorder realizations. Indeed, we see that while MC fluctuations with  $N_m = 100$  are of the same order of magnitude that sample-to-sample fluctuations, making  $N_m = 1000$  measurement steps is enough to keep MC errors much smaller than fluctuations due to random configurations. To further illustrate in a more quantitative way the fact that disorder fluctuations are much bigger than MC fluctuations, we show in Fig. 9 the full distribution of  $\ln(\rho_{\text{sf}})$  obtained for a system of linear size  $L = 16$  with  $\mathcal{N}_s \approx 20000$  samples at disorder strength  $W = 5$  (BG regime) on which we have superimposed histograms of  $\sim 300 - 400$  MC averages over  $10^3$  MC steps for 5 representative samples. Hence, it appears more efficient to perform a relatively modest number of MC steps  $\sim 10^3$ , in order to be able to sample more disorder realizations. Note that the MC error is nevertheless included in our data analysis as discussed below.



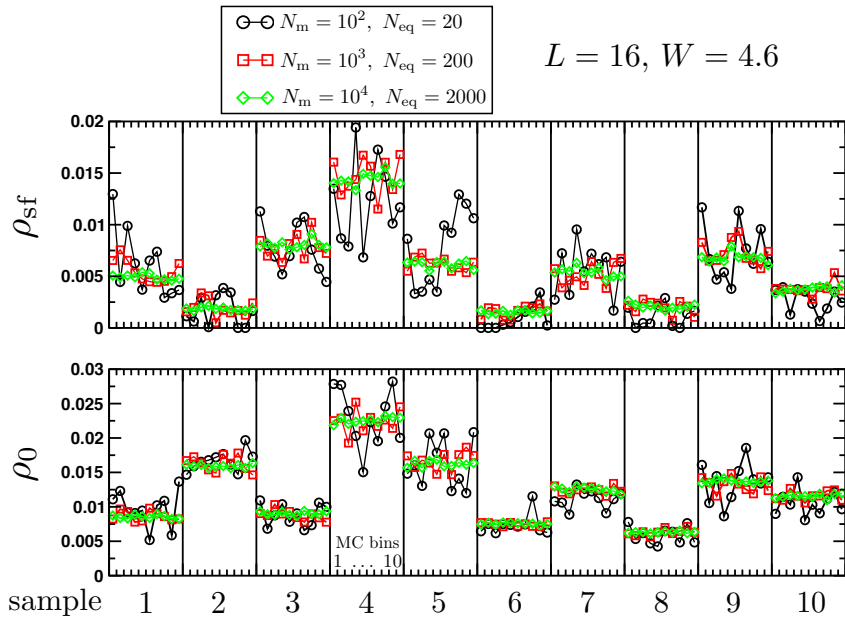


Figure 8. Example of 10 disorder realizations for a system of size  $N = 16 \times 16$  at disorder strength  $W = 4.6$  (SF regime). The upper (lower) panel shows the SF (BEC) density measured for each disordered sample with 10 independent consecutive bins, each with a different number of MC Steps  $N_m = 10^2, 10^3, 10^4$  (different symbols). It is clear that for  $N_m \geq 10^3$  the MC fluctuations are smaller than fluctuations between disordered samples.

### B. Disorder fluctuations

The problem of increasing variances in the BG phase leads to a sampling issue which can be tackled for finite

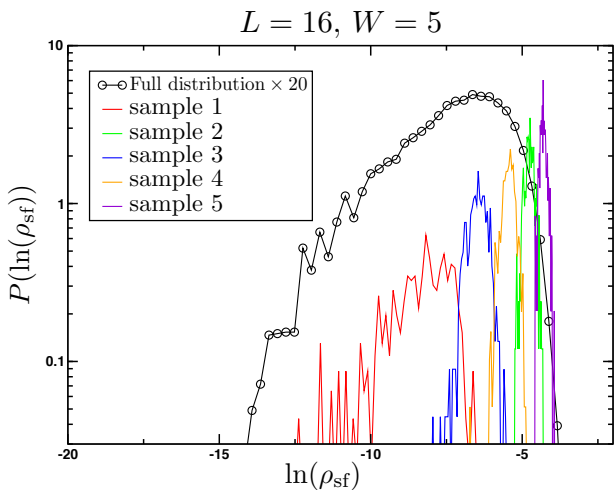


Figure 9. Distribution of  $\ln(\rho_{\text{sf}})$  for system size  $N = 16 \times 16$  at disorder strength  $W = 5$  (BG). The black circles curve is the full distribution over  $\approx 20000$  disordered samples, multiplied by a factor of 20 for graphical reasons. The colored lines are the histograms of  $\sim 300 - 400$  MC bins of  $N_m = 10^3$  steps, shown for 5 representative disordered samples. The spread of the MC bin distributions is clearly much smaller than the spread stemming from disordered samples.

systems by using a very large number of disorder realizations. In order to estimate how many samples should be used to obtain a reliable and converged result, we calculate running means as a function of the number of disorder realizations.

Figure 10 shows the estimated averages and error bars of both SF and BEC densities for increasing number of disorder realizations for different system sizes and disorder strengths. Seemingly, averages over around 1000 disorder realizations are not fully converged and for the smaller system sizes, at least some 10000 disordered samples are needed for a converged result, while for larger systems, at least 5000 disordered samples are required. To be safe, we choose to reach  $\sim 20000$  disorder realizations for the smaller sizes  $L \leq 22$  and  $\sim 10000$  for system sizes  $L \geq 24$ .

In addition, a very large number of disorder realizations are also needed to correctly sample the distributions of  $\ln(\rho_{\text{sf}})$  since they broaden with increasing system size, as shown in the main text. This further justifies our choice of such very large numbers of samples (see also Ref. [2] for a related discussion).

### C. Bootstrap analysis

For our scaling analysis of  $\rho_0$  and  $\rho_{\text{sf}}$  it is crucial to take into account the correct error bars of our results for every system size and disorder strength. While the aver-

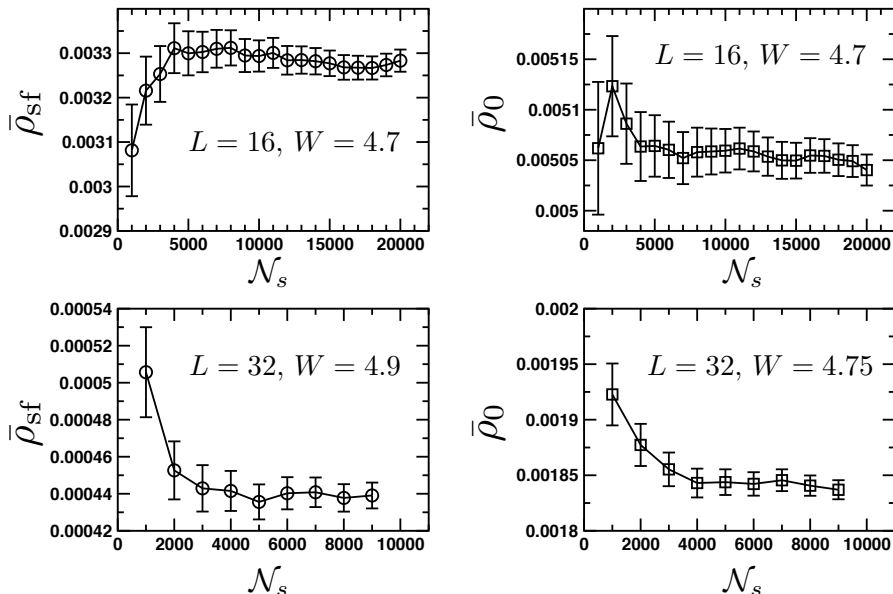


Figure 10. Disorder average of the superfluid density  $\rho_{sf}$  and the Bose condensed density  $\rho_0$  as a function of number of disorder realizations for different system sizes ( $N = 16 \times 16, 32 \times 32$ ) and disorder strengths. A number of samples  $\mathcal{N}_s \gg 10^3$  appears necessary to avoid unconverged disorder averages.

age value is simply given by the disorder average of the MC averages, the total error bar can be estimated using a bootstrap approach. For this, we generate a set of bootstrap samples by randomly selecting a subset  $\{i_B\}$  from the  $\mathcal{N}_s$  realizations with replacement (selecting in total  $\mathcal{N}_s$  realizations from the ensemble with replacement) and drawing a Gaussian random number distributed according to

$$p(x) = \frac{1}{\sqrt{2\pi}\sigma_{MC}} e^{-(x-\rho)^2/(2\sigma_{MC}^2)} \quad (7)$$

for each selected sample, which we then average over  $\{i_B\}$ . This is repeated many (typically  $\approx 1000$ ) times and the standard deviation of the result is indeed an accurate estimator of the total error bar. We have also checked that the MC error is smaller than the disorder fluctuations so that the final results are unchanged if it is neglected (see Fig. 12).

In order to determine error bars of the critical disorder strength  $W_c$  and the critical exponents, a second level of bootstrap analysis is introduced, which performs multiple fits by a gaussian resampling of our results for  $\rho_0$  and  $\rho_{sf}$  within the previously determined error bars. The standard deviation of the such obtained fit results represent the statistical error of the final results (see Fig. 12 and table II)

### III. OVERCOMING LARGE AUTOCORRELATION TIMES FOR $\rho_{sf}$

#### A. Dynamical increase of the number of MC steps

For disorder realizations which exhibit a particularly small value of the superfluid density  $\rho_{sf}$ , which is measured in the SSE by counting the winding number fluctuation of worldlines, we find that autocorrelation times become larger and the change between the 0 winding number sector to nonzero winding numbers takes more MC steps. For these cases, we decide dynamically to perform additional blocks of 1000 MC steps until the final result is reliable and the total simulation time is much longer than the autocorrelation time, involving simulations with up to  $10^5$  MC steps. This method gives reliable access to small values of  $\rho_{sf}$ , which would be estimated to be 0 otherwise, which is not expected for our finite size samples.

We set the  $10^5$  MC steps limit for computing time reasons and the rare disorder realizations needing more steps are evaluated to zero stiffness. These realizations cannot be used for the discussion on the distributions of  $\ln(\rho_{sf})$ , nor the typical stiffness. However, they can be included in the calculation of the average stiffness as neglecting them would induce systematic errors. In fact, our analysis leads us to speculate that these samples have been simulated at a too high temperature and are not converged to the GS.

There are several possibilities which we all explored

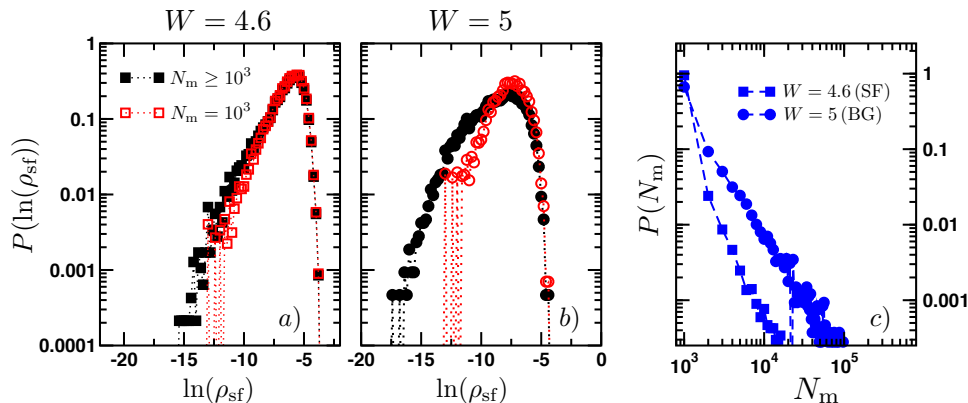


Figure 11. Histogram of  $\ln(\rho_{\text{sf}})$  in SF (panel a) and BG (panel b) phase for a system of size  $N = 24 \times 24$  when the number of MC steps is fixed to  $10^3$  (red) and when it is dynamically adjusted as described in the text (black). c) Fraction of disorder realizations having needed  $N_{\text{mc}}$  Monte Carlo steps for the same system size and disorder strengths.

and found little dependence of our results on the particular choice. *i)* Adding samples of vanishing  $\rho_{\text{sf}}$  to the data set and performing the data analysis described before. This corresponds to approximating the distribution of  $\rho_{\text{sf}}$  by a distribution with a cut-off at the minimal stiffness observed in the ensemble and a delta peak at zero. Clearly this is an incorrect estimation as the correct distribution vanishes at zero and the delta peak is both due to insufficient simulation time and too high temperature, thus introducing a (small) systematic error. *ii)* Extrapolation of the distributions of  $\ln(\rho_{\text{sf}})$  towards zero by a power law tail (straight line in the plots in figure 11) but since this is the least properly sampled part of the distribution a reliable extrapolation cannot be achieved. *iii)* The replacement of the non physical zero values by half the value of the cut-off (*i.e.* the minimal computed stiffness for every couple  $(L, W)$ ). This corresponds to approximating the small  $\rho_{\text{sf}}$  tail of the distribution by a box distribution and is only justified by the very small weight of the approximated part of the distribution. We used this last solution for checking the stability of our scaling analysis and found that our results are not dependent on whether these samples are included or not. Hence, to treat on equal footing the typical and average stiffness, we decided to neglect them, as the introduced bias is much smaller than our overall uncertainty.

Future work could try to adress this problem by investing more computer time in samples with small values of  $\rho_{\text{sf}}$ . We have found that these samples are typically not completely converged in the GS and it should be explored if one can solve the problem by reducing the temperature iteratively in such samples.

### B. Improved sampling of the full stiffness distributions

A comparison of results obtained with only  $N_m$  fixed to 1000 MC steps to results obtained with our dynamic Markov chain length method are displayed in Fig. 11 for a system in the SF (though strongly disordered) regime (panel a) and inside the BG phase (panel b). It is clear that our dynamical adjustment of the MC steps allows for much smaller SF stiffnesses to be computed, especially inside the BG phase. The implementation of this procedure allows for the distribution of  $\ln(\rho_{\text{sf}})$  to be accurately sampled and hence, for an appropriate estimation of the standard deviation of  $\ln(\rho_{\text{sf}})$ . Without this method, the broadening of the distributions for growing system sizes inside the BG phase (described in the main text) could not have been investigated quantitatively, nor even qualitatively observed.

## IV. CRITICAL EXPONENTS

$L_{\text{min}}$	$Q_0$ ( $\times 100$ )			$Q_{\text{sf}}$ ( $\times 100$ )		
	[4.6; 5]	[4.65; 5]	[4.7; 5]	[4.6; 5]	[4.65; 5]	[4.7; 5]
12	8.7	13.3	16.2	4.5	4.25	11
16	7	15.2	13.5	4	5	9.2
20	21.3	39.75	33.8	37.5	39.25	39.5

Table II. Quality of the fits of the critical parameters from the Bose condensed density ( $Q_0$ ) and from the superfluid density ( $Q_{\text{sf}}$ ), corresponding to the parameters shown in table 1 in the main text and figure 12 for different windows of disorder and of system size  $[L_{\text{min}}; 32]$ .

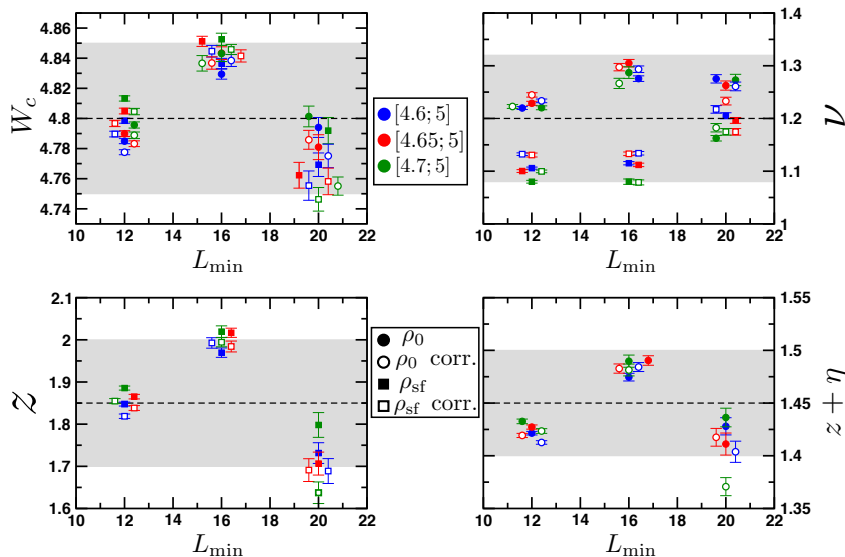


Figure 12. Bootstrap estimates of the critical exponents for different disorder and system size windows. Different colors represent the estimates for different windows of disorder. Circles depict estimates obtained with the scaling of the BEC density  $\rho_0$  and squares those obtained via the superfluid density  $\rho_{sf}$ . Full symbols correspond to critical parameter estimates when no systematic error correction is added and open symbols estimates where both the Monte Carlo and temperature systematic error corrections are included. The dashed line gives the final best estimate and the shaded area the final uncertainty.

We have discussed above how the statistical error on the critical disorder strength and the critical exponents may be obtained. However, we believe that the systematic error due to small system sizes which may require corrections to scaling in our scaling analysis is in fact dominant, as results change slightly if the size of the fit window in system size or included disorder strengths is varied.

Therefore, we have performed a systematic analysis of this systematic error and give error bars that represent the total fluctuation of our results. This is represented in Fig. 12.

In order to quantify the quality of our fits, we calculate the sum of squared residuals

$$\chi^2 = \sum_i \left( (\rho_{sf|0}^i - \text{fit}(W_i, L)) / \sigma_i \right)^2 \quad (8)$$

and obtain the probability  $Q$  of finding a  $\chi^2$  greater or equal than this value given the fit by

$$Q = \frac{1}{\Gamma(n_{\text{dof}}/2)} \int_{\chi^2/2}^{\infty} dy y^{n_{\text{dof}}/2-1} e^{-y}, \quad (9)$$

as explained in Ref. 3.

The corresponding qualities of fit  $Q$  for each window in size and included disorder strengths are shown in table II. There are two reasons why the qualities of fit are systematically larger for the window [20; 32]. First, reducing the number of system sizes included in the analysis while

keeping the bigger sizes means that there is less size dynamics, hence the fact that no drift term is included in the fits becomes more justified. Secondly, the bigger system sizes have slightly bigger relative error bars so the corresponding  $\chi^2$  is smaller and the quality of fit  $Q$  larger as these two quantities are very sensible to the error bars. Consequently, we treat all fit windows on equal footing to estimate averages and uncertainties and do not give a bigger weight to the estimates obtained with  $L_{\min} = 20$ .

In figure 12 we plot the critical parameters with their error bars, obtained from a bootstrap analysis with 100 bootstrap samples, for every window in system size and included disorder strength corresponding to table II. For comparison, the critical exponents and critical disorder strength estimates, with their error bars, given upon including the corrections to the systematic errors due to temperature convergence and the Monte Carlo error bars are also shown (open symbols). It is clear that including the correction of the possible systematic errors does not change the final estimations of the critical parameters as well as their error bars, which are quite large.

- 
- [1] A. W. Sandvik *Phys. Rev. B* **66**, 024418 (2002).
  - [2] F. Lin, E. S. Sørensen, and D. M. Ceperley, *Phys. Rev. B* **84**, 094507 (2011).
  - [3] P. Young, *arXiv e-print* 1210.3781 (2012).